Biomedical Optics EXPRESS

# Sequential average segmented microscopy for high signal-to-noise ratio motion-artifact-free *in vivo* heart imaging

**Claudio Vinegoni,[1,4,*] Sungon Lee,[1,2,4] Paolo Fumene Feruglio,[1] Pasquina Marzola,[3] Matthias Nahrendorf,[1] and Ralph Weissleder[1]**

[1]*Center for System Biology, Massachusetts General Hospital and Harvard Medical School, Richard B. Simches Research Center, 185 Cambridge Street, Boston 02114, USA*

[2]*Interaction and Robotics Research Center, Korea Institute of Science and Technology, Hwarangno 14-gil 5, Seongbuk-gu, Seoul, South Korea*

[3]*Department of Computer Science, University of Verona, Strada le Grazie 15, I-37134 Verona, Italy*

[4]*Equal contribution*

[*]*cvinegoni@mgh.harvard.edu*

**Abstract:** *In vivo* imaging is often severely compromised by cardiovascular and respiratory motion. Highly successful motion compensation techniques have been developed for clinical imaging (e.g. magnetic resonance imaging) but the use of more advanced techniques for intravital microscopy is largely unexplored. Here, we implement a sequential cardiorespiratory gating scheme (SCG) for averaged microscopy. We show that SCG is very efficient in eliminating motion artifacts, is highly practical, enables high signal-to-noise ratio (SNR) *in vivo* imaging, and yields large field of views. The technique is particularly useful for high-speed data acquisition or for imaging scenarios where the fluorescence signal is not significantly above noise or background levels.



**OCIS codes:** (180.0180) Microscopy; (170.2520) Fluorescence microscopy; (170.5810) Scanning microscopy; (170.3880) Medical and biological imaging.

## References and links

1. R. Weigert, M. Sramkova, L. Parente, P. Amornphimoltham, and A. Masedunskas, "Intravital microscopy: a novel tool to study cell biology in living animals," Histochem. Cell Biol. **133**(5), 481–491 (2010).
2. M. J. Pittet and R. Weissleder, "Intravital imaging," Cell **147**(5), 983–991 (2011).
3. P. Bousso and H. D. Moreau, "Functional immunoimaging: the revolution continues," Nat. Rev. Immunol. **12**(12), 858–864 (2012).
4. L. Ritsma, B. Ponsioen, and J. van Rheenen, "Intravital imaging of cell signaling in mice," Intravital **1**(1), 2–8 (2012).
5. S. Yazdanfar, M. Kulkarni, and J. Izatt, "High resolution imaging of *in vivo* cardiac dynamics using color Doppler optical coherence tomography," Opt. Express **1**(13), 424–431 (1997).
6. S. Lee, C. Vinegoni, P. F. Feruglio, L. Fexon, R. Gorbatov, M. Pivoravov, A. Sbarbati, M. Nahrendorf, and R. Weissleder, "Real-time *in vivo* imaging of the beating mouse heart at microscopic resolution," Nat Commun **3**, 1054 (2012).
7. M. R. Looney, E. E. Thornton, D. Sen, W. J. Lamm, R. W. Glenny, and M. F. Krummel, "Stabilized imaging of immune surveillance in the mouse lung," Nat. Methods **8**(1), 91–96 (2011).
8. S. Laffray, S. Pagès, H. Dufour, P. De Koninck, Y. De Koninck, and D. Côté, "Adaptive movement compensation for *in vivo* imaging of fast cellular dynamics within a moving tissue," PLoS ONE **6**(5), e19928 (2011).
9. R. T. A. Megens, S. Reitsma, L. Prinzen, M. G. oude Egbrink, W. Engels, P. J. Leenders, E. J. Brunenberg, K. D. Reesink, B. J. Janssen, B. M. ter Haar Romeny, D. W. Slaaf, and M. A. van Zandvoort, "*In vivo* high-resolution structural imaging of large arteries in small rodents using two-photon laser scanning microscopy," J. Biomed. Opt. **15**(1), 011108 (2010).
10. A. D. Scott, J. Keegan, and D. N. Firmin, "Motion in cardiovascular MR imaging," Radiology **250**(2), 331–351 (2009).
11. J. Tsao and S. Kozerke, "MRI temporal acceleration techniques," J. Magn. Reson. Imaging **36**(3), 543–560 (2012).

#189045 - $15.00 USD Received 13 May 2013; revised 5 Aug 2013; accepted 6 Aug 2013; published 9 Sep 2013

12. D. J. Atkinson and R. R. Edelman, "Cineangiography of the heart in a single breath hold with a segmented turboFLASH sequence," Radiology **178**(2), 357–360 (1991).
13. J. P. Finn and R. R. Edelman, "Black-blood and segmented k-space magnetic resonance angiography," Magn. Reson. Imaging Clin. N. Am. **1**(2), 349–357 (1993).
14. T. K. Foo, M. A. Bernstein, A. M. Aisen, R. J. Hernandez, B. D. Collick, and T. Bernstein, "Improved ejection fraction and flow velocity estimates with use of view sharing and uniform repetition time excitation with fast cardiac techniques," Radiology **195**(2), 471–478 (1995).
15. S. Lee, C. Vinegoni, P. F. Feruglio, and R. Weissleder, "Improved intravital microscopy via synchronization of respiration and holder stabilization," J. Biomed. Opt. **17**(9), 096018 (2012).
16. M. B. Bernstein, K. F. King, and X. J. Zhou, *Handbook of MRI pulse sequences* (Elsevier Academic Press, 2004).
17. R. H. Hashemi, W. G. Bradley, and C. J. Lisanti, *MRI: The Basics* (Lippincott Williams &Wilking, 2010).

## 1. Introduction

Fluorescence microscopy has broadened our understanding of biological life, offering novel insights into physiological and pathological processes. High penetration depth, low phototoxicity, high spatial and temporal resolution, have all contributed to making confocal and multiphoton laser scanning fluorescence microscopy extremely successful, particularly for *in vivo* applications. Now, following the development of window chambers, and with easier access to the chest or abdominal cavities for organ imaging, intravital microscopy (i.e. live animal imaging at microscopic resolution [1, 2]) offers the invaluable advantage of providing cellular information under natural physiological conditions, unlike observations using conventional *in vitro* culture models, which often fail to correlate with *in vivo* results. Intravital microscopy is thus an indispensable tool for studying the micro-dynamics of biological processes. Indeed, recently, building upon technological developments in related areas, microscopy has started to address longstanding questions in cell biology, neurobiology, immunology, and tumor biology [1–5].

One critical issue faced by all *in vivo* imaging techniques, however, is the fact that measurements can be severely hampered by movement of the imaged tissue. This is particularly problematic when using scanning-like techniques such as fluorescence laser scanning microscopy (LSM) [6–9]. In these techniques, a laser excitation scanning point draws a continuous raster path within the selected field of view (i.e. individual pixels within an image are all acquired at different points in time). Unfortunately, physiological tissue motion, primarily from cardiac contraction and respiration, often gives rise to artifacts, which can vary in severity depending on the imaged organ and on the selected acquisition parameters (e.g., integration time and resolution).

To date, various motion reduction methods have been developed for magnetic resonance imaging (MRI), particularly for high resolution cardiac MRI [10, 11]. While the basic imaging principles of MRI and optical microscopy are different, the principles of image stabilization are adaptable to both techniques. Herein, we thus introduce a technique known as sequential cardiorespiratory gating (SCG) segmented average microscopy, a stabilization method that is commonly used for cardiac MRI [12–14]. We consequently show how its implementation, when used in combination with a custom made tissue stabilizer, enables highly stable and reproducible *in vivo* heart imaging with high SNR. The technique we propose is based on an acquisition methodology that we originally applied to *in vivo* heart imaging of structures with high fluorescence signal content [6]. The strategy presented in the current study, however, now extends this method to imaging scenarios where there is very low fluorescence signal or where the background signal is of comparable intensity to the fluorescent target. These types of situations can occur for a variety of different reasons such as when there is low endogenous fluorescent protein expression, or modest probe accumulation. The strategy could also be useful for imaging samples that need to be illuminated with low power excitation to avoid photobleaching and/or decrease phototoxicity during longitudinal studies. Finally, during fast imaging acquisitions at video frame rate, the reduced dwell time can severely degrade the quality of images, and thus result in lower total

#189045 - $15.00 USD Received 13 May 2013; revised 5 Aug 2013; accepted 6 Aug 2013; published 9 Sep 2013

image SNR. The proposed technique, which uses a sequential average segmented methodology to average over multiple image segments, now offers the ability to increase the quality (SNR) of reconstructed images for all scenarios, and to produce low noise, motion-artifact-free images.

## 2. Motion compensation scheme for cardiac imaging in MRI and LSM

Raw data sets in Fourier transform MRI consist of a complex matrix acquired in the k-space. Figure 1 illustrates the experimental approach and highlights the differences and similarities between motion compensation in MRI and optical microscopy for cardiac imaging.

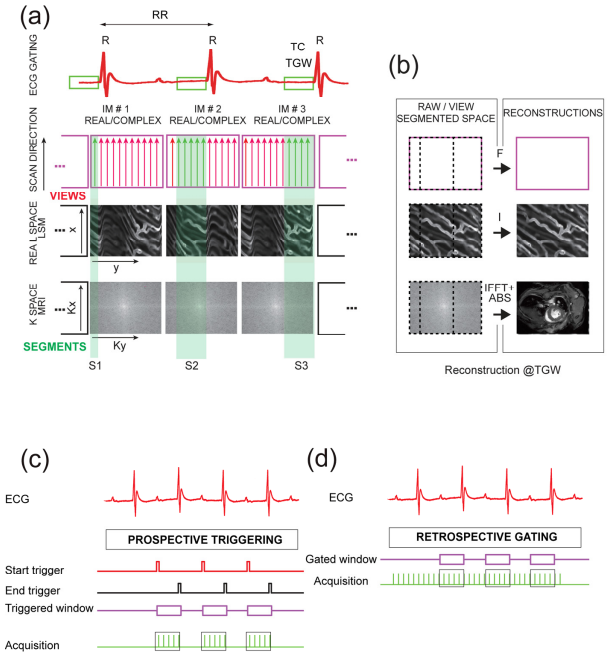


Fig. 1. Scheme of principle for sequential retrospective electrocardiogram (ECG)-gated segmented microscopy. For figure simplicity, we assume here the absence of any respiratory motion. (a) In MRI, a sequence of views is collected in the k-space, by varying the phase encoding gradient. Laser scanning microscopy (LSM) images (IM) are acquired pixel by pixel in the real space, with the excitation scanning laser beam moving along a predefined path (MRI analogue of a group of views). Groups of views (segments S1, S2, etc.) are sequentially collected within a time-gated window $T_{GW}$, which is coincident with the time window $T_C$, corresponding to the end-diastole. The QRS complex, groups all waves within an ECG generated during ventricular depolarization. R indicates the R phase of the QRS complex. The process is then repeated until the entire real space (LSM) or k-space (MRI) is filled. (b) Image reconstructions are obtained by grouping several consecutive segments and by then transforming them using the function F. In MRI, an image is obtained by applying a transformation (the inverse Fourier transformation IFFT in conjunction with the absolute function ABS (i.e., IFFT + ABS), to each pixel of the image matrix. In LSM, images are constructed directly in the real space and the transformation does not induce any further change after grouping. F can therefore be considered as the identity function (I). (c) Prospective triggered acquisition scheme: data for images are acquired only during the time of a specific triggered window, which is determined by ECG. All acquired data are therefore used for image reconstruction. (d) Retrospective gated acquisition scheme: data for images are continuously acquired together with the ECG recording. Following this non-selective acquisition, only the data that were acquired during the time of a specific gated window, which is determined by ECG, are chosen for image reconstruction. RR indicates the distance between two R phases. IM indicates a generic image.

#189045 - $15.00 USD Received 13 May 2013; revised 5 Aug 2013; accepted 6 Aug 2013; published 9 Sep 2013

During MRI acquisition, each matrix row ("view") of the raw data set corresponds to a specific magnetic resonance (MR) signal acquired under a certain intensity of the phase encoding gradient. The required number of MRI signals necessary to build an image, each representing one row of the data matrix, are then acquired sequentially and individually to cover the entire matrix. This type of acquisition modality is also known as "line-by-line", or alternatively as "view per view" acquisition (Fig. 1(a)). While the two-dimensional Fourier transform of the data matrix provides the complex image in the real space, standard MR images are obtained by calculating the absolute value of the complex numbers.

MRI, however, is profoundly and fundamentally different to LSM. Namely, the former works in the complex (Fourier) domain (k-space) while the latter works in the real domain. Nevertheless, despite their differences, some analogies can be drawn between the two modalities in terms of data acquisition, particularly when considering the problem of image acquisition acceleration and motion compensation. These analogies thus allow us to implement some of the strategies commonly used in MRI to obtain motion-artifact-free images using LSM.

First, for both modalities, volumetric information is obtained through simple superimposition of planar images acquired at different depths (slices). Specifically, MRI uses a magnetic field with linearly increasing magnitude along the slice direction in combination with pulsed radio frequency electromagnetic stimulation, to extract virtual slices through an imaged sample. This virtual slicing or segmentation is similar for LSM, but is "optical" in nature rather than "magnetic". Here, a pinhole placed close to the photodetector rejects photons emanating from fluorophores and/or from fluorescent proteins that belong to planes above or below the objective's focal plane.

Second, in standard MRI, the different lines of the k-space are sequentially and individually acquired starting from the periphery, with the total acquisition time governed by the time interval between the acquisition of two views (pulse sequence repetition time, $T_{Rep}$) multiplied by the number of the views $N$ required to fill the k-space matrix ($N*T_{Rep}$). Similarly, in LSM, different lines of the image real space are also sequentially and individually acquired. During LSM acquisition, the laser excitation scanning point draws a continuous raster path along a predefined pattern with a periodicity $T_L$, determined by the line scanning time. The fluorescence signal is then detected by a photodetector and sampled at a certain frequency, which is equal to the inverse of the dwell time or pixel integration time.

Finally, because MRI works in the k-space, images are not collected directly e.g., by acquiring a group of pixels, but are instead reconstructed from two-dimensional Fourier transformations (Fig. 1(a)). The collection of different signals, by varying the phase encoding gradient intensity, thus allows the acquisition of different views, and representative image can be reconstructed after inverse Fourier transformation (Fig. 1(b)). In LSM, single lines are sampled directly in the real space (Fig. 1(a)). By collecting all the different pixel intensities, a two-dimensional matrix, i.e., an image, is obtained. Each row in the LSM image can thus be seen as equivalent to a line in the k-space (or view) of the MR image, even though they are operating in a different space domain (Fig. 1(b)).

Both MRI and LSM can be used for sequential acquisition. This form of acquisition technique, however, can be prohibitively time consuming when imaging dynamic events such as the arrival of a contrast agent in tissues, or when imaging a fast moving object such as a beating heart. Longer acquisition times can also lead to severe consequences in terms of image artifacts. In LSM, for example, to scan a single image, the excitation laser scanning point has to move along a pre-defined trajectory across a horizontal imaging plane. Consequently, because of motion components induced by cardiac and respiratory activities, not all points along this trajectory will lie at the same depth within the imaged organ [15]. As a result, the acquired image will not correspond to a horizontal imaging plane sectioned across the sample but will instead be a representation of a more complex (curved) surface whose profile is weighted by the speed of the motion and the acquisition parameters [16].

#189045 - $15.00 USD Received 13 May 2013; revised 5 Aug 2013; accepted 6 Aug 2013; published 9 Sep 2013

Since breathing and cardiac motion cause imaged areas to move in an irregular pattern, different regions of an acquired image will appear more or less blurred as the local displacement (between the focal plane and the sample) increases as a function of time. For example, in cardiac imaging, data acquired during the time window $T_{GW}$ corresponding to the end-diastole (Fig. 1(a)), a cardiac phase in which the heart is in a resting state, have minimal motion induced distortion.

To overcome this problem of motion artifacts and distorted images, a variety of techniques have been developed to date that speed up scanning acquisition times for MRI, and/or involve the use of temporal or spatiotemporal redundancy [10–14]. In general, the key principle underlying scan acceleration is based on the presence of quasi-periodic motion components. Namely, the predictable reproducibility or similarity of tissue position at certain time points during biological (cardiac and respiratory) cycles enables assisted motion-synchronized scanning [11]. Consequently, by using *a priori* knowledge in combination with prospective triggering or retrospective gating, it is possible to image fast moving objects.

## 3. Methods

Sequential 'segmented cardiac-gated MRI' is an acquisition modality commonly used to overcome physiological motion components [12, 13]. This modality was introduced approximately two-decades ago and has been extensively used for cardiac MRI. In the present application, an electrocardiogram (ECG)-triggered sequential acquisition was used to acquire identical pulse sequences (Fig. 1(c)). Namely, a specific slice was excited to acquire a particular group of views ("segment") S1 [16,17] within each R-R time interval i.e., the time period between one R wave and a subsequent R wave in a sequential cardiac cycle (Fig. 1(a)). Following the acquisition of S1, a different segment S2 within the same slice was measured and the process repeated until the entire k-space was filled. Due to the quasi-periodicity and reproducibility of the cardiac motion, complete k-space images could be reliably reconstructed by grouping segments acquired at different times within a defined period of the cardiac cycle in the ECG, i.e., within a defined cardiac phase.

A slightly different version of the same technique can be performed using retrospective gating (Fig. 1(d)). This technique does not require the ECG signal to trigger MRI acquisition. Instead, ECG signals are measured continuously during MRI acquisition, without any time relationship between the onset of MRI acquisition and the ECG signal. Post-processing retrospective ECG-gating is then performed, where for each image only the k-space lines acquired during well–defined similar time intervals within the cardiac cycle (ECG) are retained. These are subsequently grouped such that a complete k-space image can be obtained (see Fig. 1).

The above-described acquisition technique can be easily extended to LSM (Figs. 2 and 3). In this case, by grouping views into segments, gated according to specific time points within the ECG, a final representative image of a tissue during a particular cardiac phase can be reconstructed (Fig. 1(b)). For simplicity reasons, let us consider only the cardiac motion component. When we choose a time-gated window $T_{GW}$ coincident with the time window $T_{C,}$ corresponding to the end-diastole (i.e., where the heart is in a relaxed state), all acquired segments will be representative of the same horizontal physical plane (heart at rest), and will thus exhibit minimal distortion. If we would have chosen a time-gated window positioned at another time different from $T_C$ all acquired segments would have been representative of a complex (curved) surface with a profile weighted by both heart contractions, and the acquisition parameters.

#189045 - $15.00 USD Received 13 May 2013; revised 5 Aug 2013; accepted 6 Aug 2013; published 9 Sep 2013

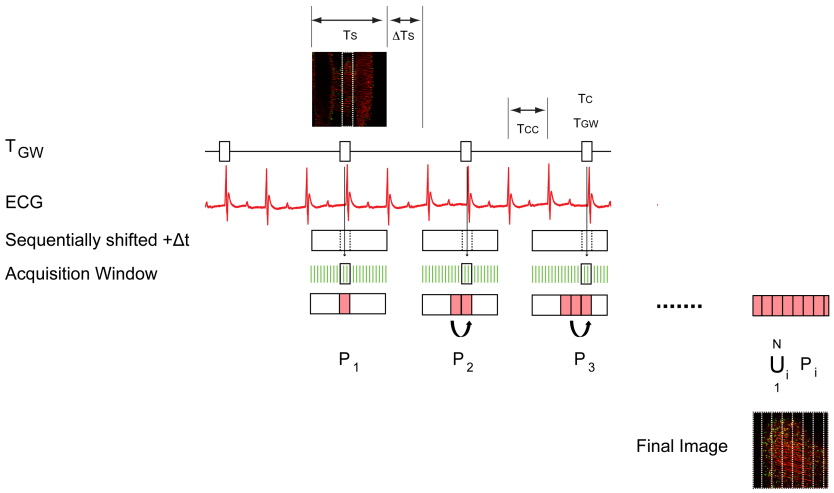


Fig. 2. Timing diagram and image reconstruction scheme for non-averaged microscopy in sequential retrospective cardiac-gated segmented microscopy. For the sake of simplicity we assume the absence of any respiratory motion in both time diagrams. We define as $T_{CC}$ the time interval between two cardiac cycles, as $T_S$ the acquisition time of a single raw image, as $\Delta T_S$ the time interval between the end and the beginning of two consecutive acquisitions, and as $T'_s = T_s + \Delta T_S + \Delta T_S$ the time interval between two consecutive images. Sequentially time-shifted images ($\Delta t = T_{GW}$) were acquired, and $N$ individual segments $P_i$ (shown in red) within each image were isolated (corresponding to the time-gated window $T_{GW}$). Segments were then grouped together ($\bigcup_{1}^{N} P_i$) and a final image was reconstructed. The reconstructed image thus provides a true representation of the heart's morphology (i.e., a flat virtual section) at the cardiac phase corresponding to the time-gated window $T_{GW}$. In order to simply illustrate the concept of segmented microscopy we have assumed that the cardiac cycle is constant and that $T'_s = nT_{CC} - T_{GW}$. This implies that the segmented areas from consecutive images will be adjacent to each other.

As outlined in the introduction we are interested in averaging over multiple image segments, in order to increase the SNR of the reconstructed images such that we can obtain low noise, motion-artifact-free images. One major hamper, however, is the fact that LSM generally operates at a higher resolution than MRI. Therefore during acquisition any kind of slight misalignment between each individual segment corresponding to the same part of the final image could lead to blurring or distortion artifacts during the averaging process. It is therefore extremely important, when averaging and grouping segments, that all motion components are highly reproducible, to ensure that segments collected at different time points (but belonging to the same specific phase of the cardiac cycle) will be equal to each other over time. If segments lack reproducibility, even if gating is applied, images will no longer be representative of the same imaging plane within a tissue. Consequently, using such data and averaging over multiple segments, will lead to blurry reconstructed images.

#189045 - $15.00 USD Received 13 May 2013; revised 5 Aug 2013; accepted 6 Aug 2013; published 9 Sep 2013

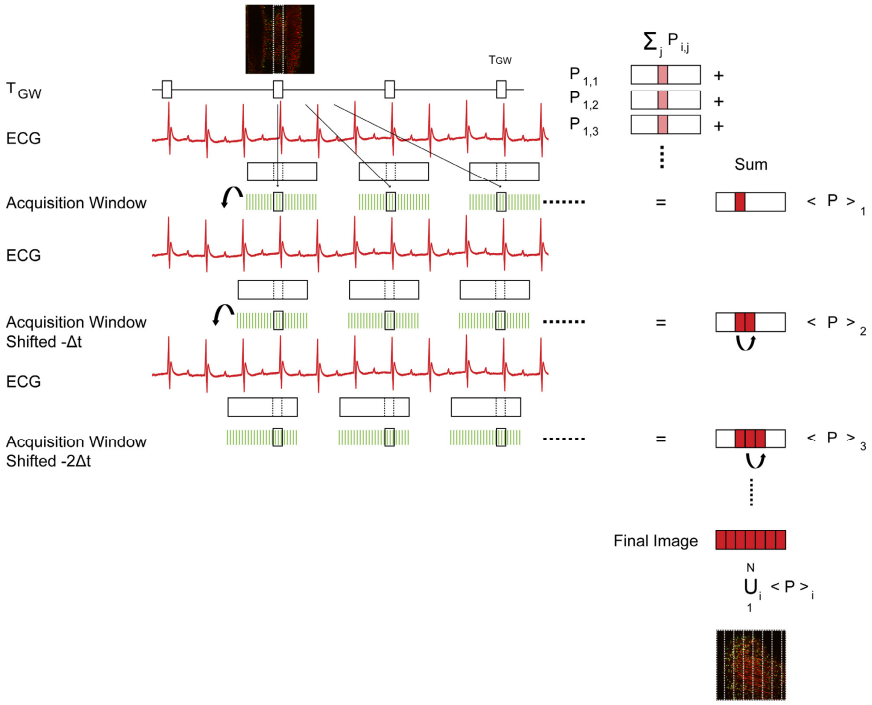


Fig. 3. Timing diagram and image reconstruction scheme for averaged microscopy in sequential retrospective cardiac-gated segmented microscopy. Data acquisition was initiated at a specific phase of the cardiac cycle, and $M$ identical segments $P_{i,j}$ within the time gated window $T_{GW}$ were then extracted from each image. A 'summation segment' $< P >_1$ was obtained by merging all the segments ($< P >_1 = \sum_{1}^{M} P_{1,j}$). To simply illustrate the concept of segmented averaging microscopy we assume that the cardiac cycle is constant and that $T'_S = nT_{CC}$. This implies that segmented areas from consecutive images will be overlapping on each other in order to obtain an average segment. Data acquisition was subsequently initiated at a different phase of the cardiac cycle, time shifted according to the quantity of $T_{GW}$ from the first acquisition such that $T'_s = nT_{CC} - T_{GW}$, and a second 'summation segment' $< P >_2$ obtained. The process was repeated multiple times ($N$) until the 'summation segments' covered the entire image field to render a final image with high SNR ($\bigcup_{1}^{N} < P >_i$).

In a bid to reduce the amplitude motion range from millimeters to microns and to enhance motion reproducibility across all cardiac cycles, we recently developed a strategy that makes use of a custom made holder for mechanical tissue stabilization [6]. By increasing reproducibility, the stabilizer in combination with segmented acquisition at specific cardiac and respiratory phases, enables both prospective and retrospective gating approaches to be applied. Segments corresponding to the same physiological time point within the cardiac cycle over time (Fig. 3) are thus highly correlated without or with minimal border discontinuities. This in turn ensures favorable conditions for the performance of *in vivo* sequential cardiac- and respiratory-gated (both non-averaged Fig. 2 and averaged Fig. 3) segmented microscopy. In using this approach, individual segments are repeatedly collected and then merged together to increase the SNR not only of each segment but also of the final reconstructed image.

#189045 - $15.00 USD Received 13 May 2013; revised 5 Aug 2013; accepted 6 Aug 2013; published 9 Sep 2013

## 4. Experimental setup

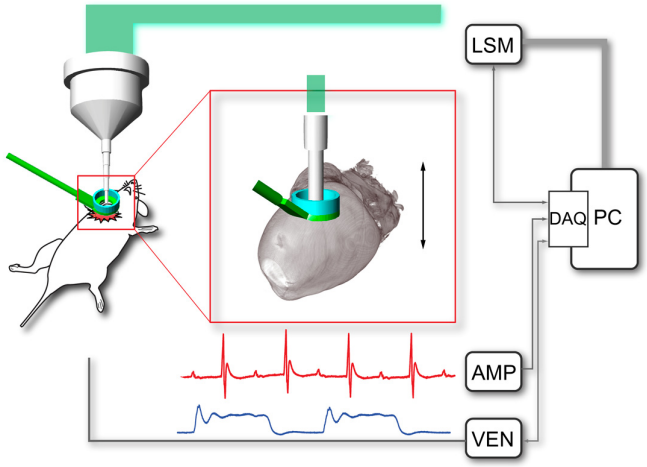


Fig. 4. Experimental setup. LSM, laser scanning microscope; DAQ, data acquisition card; AMP, differential amplifier; VEN mechanical ventilator. Inset: position of stabilizing holder. LSM image acquisition was synchronized with cardiac and respiratory motion, with a DAQ-card registering the signals from the ECG amplifier and a ventilator controling the lung airway pressure.

The experimental setup is illustrated in Fig. 4, and is analogous to the setup described in detail in [6]. A custom-made stabilization holder (previously described in [6]) is used in combination with a commercial laser scanning microscope (FV1000-MPE, Olympus) and an animal mechanical ventilator (INSPIRA ASV 55-7058, Harvard Apparatus). The stabilizer consists of a ring (3.6 mm outer diameter) attached to a rigid metal shaft. The underside of the ring is coated with a thin layer of a clinical bonding agent (Dermabond) and this is gently attached to the organ of interest. The rigidity of the metal shaft ensures a substantial reduction in the amplitude of motion of the imaged organ, which can range from a few tens of microns up to a few millimeters. It also promotes reproducibility in the organ's position over time. The mechanical animal ventilator controls the frequency and amplitude of the respiratory pattern in a reproducible manner. Scanning data acquisition is thus synchronized with cardiac and respiratory motion, with a DAQ-card (PCI-6259 NI) registering the signals from the ECG amplifier (amplified using a differential pre-amplifier; DP-301 ADInstruments) and a ventilator controlling the lung airway pressure. Mice were anesthetized with isoflurane (2% in 2 L/minute oxygen). After undergoing tracheal intubation, mice were ventilated with volume control ventilation (20 ml/stroke), at a rate of 134 breaths per minute to stabilize respiration. Mice were maintained at 37.5°C throughout the procedure using a heated pad.

## 5. Results and discussion

For the sake of simplicity, the schemes of principle in Figs. 2 and 3 show retrospective gating at a specific cardiac phase, while assuming no respiratory motion. This means that the time-gate acquisition window $T_{GW}$ is constant in length over time. In reality, however, the situation is more complicated, and both cardiac and respiratory motion components need to be taken into consideration. A timing diagram for synchronizing both cardiac and respiratory motion for retrospective gated imaging is illustrated in Fig. 5 instead.

#189045 - $15.00 USD Received 13 May 2013; revised 5 Aug 2013; accepted 6 Aug 2013; published 9 Sep 2013

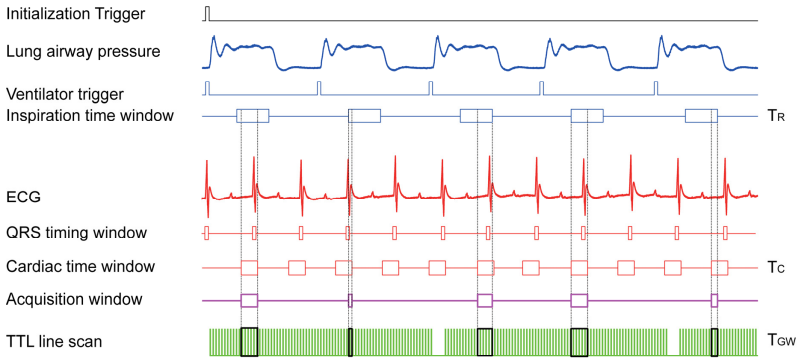


Fig. 5. Timing diagram for retrospective gated imaging. Initialization and subsequent ventilation triggers are shown in combination with the measured ECG signal and the recorded lung airway pressure. Inspiration time windows $T_R$, and cardiac time windows $T_C$ are located at points of minimum displacement for both motions. The acquisition window $T_{GW}$ corresponds to the intersection between the cardiac time window and the inspiration time windows $T_C$ and $T_R$. To note how the length of each time-gate acquisition window $T_{GW}$ is not constant but varies along time. This is independent from the specific (prospective or retrospective) imaging modality but depends only on the physiological parameters. Segments corresponding to these acquisition windows were taken from raw images.

During data acquisition, the lung airway pressure was monitored and a time window $T_R$ was individuated near the end of the inspiration or expiration phases. During the cardiac cycle, a time window $T_C$ was chosen, following the appearance of the P wave at end-diastole. Both these timing windows are located at points of minimum motion within the lungs and heart respectively. For this case (i.e. presence of respiratory and cardiac motion) the acquisition window $T_{GW}$, which is defined as the intersection between the two timing windows $T_C$ and $T_R$, thus corresponds to a concurrent temporal period in which the motion of both organs is at a minimum. All segments within this time window were then collected. The size of the new defined time-gate acquisition window $T_{GW}$ is actually irregular due to the fact that heart beat and respiration rates are different, are not in synch and/or they are not in exact multiples of each other. This is independent on the acquisition modality and holds true for both prospective and retrospective acquisition. Thus, the number of images required to collect sufficient segments as to build a stabilized image is dependent on the acquisition parameters (number of lines, pixel per lines, dwell time) as well as on their relationship to physiological parameters (heart rate, ventilator breathing frequency).

#189045 - $15.00 USD Received 13 May 2013; revised 5 Aug 2013; accepted 6 Aug 2013; published 9 Sep 2013

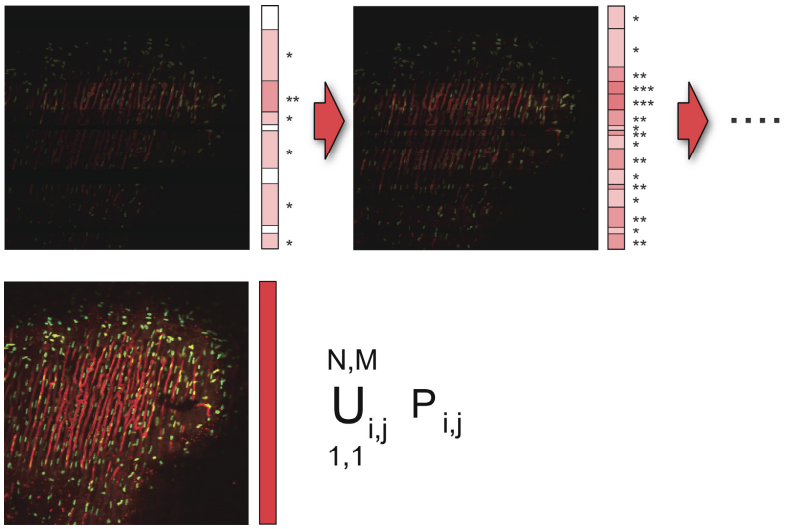


Fig. 6. *In vivo* heart imaging using sequential cardiac- and respiratory-gated average segmented microscopy. Images (left to right) illustrate how a sequential average segmented scheme improves the SNR of images. Here, specific raw data segments, corresponding to the gated time window $T_{GW}$, were collected and added (at its correct temporal position) to the reconstructed image (a summation of all previous data). The accumulation of segments continued until the number of the summation of all views (or segments) in the reconstructed image reached a predefined value. The summation of seven segments is shown. The intensity of the red color and the number of asterisks on the right side of each image represent how many segments have been summed. Fluorescence staining of myocyte nuclei is shown in green (Hoechst 33258); fluorescence lectin staining of the myocardium capillaries is shown in red (Rhodamine labeled Griffoniasimplicifolia lectin, RL-1102, Vector Laboratories). Nuclei in the middle of the image look elongated because the optical imaging plane is sectioning the heart at a different height with respect to the border area due to the natural curved surface of the heart. Cells in the center are representative of myocytes within the tissue, and are surrounded by a rich vasculature network and elongated along the axis of the microcapillaries, as opposite to the nuclei of the cells present in the border area which reside on the surface of the heart.

*In vivo* imaging of the heart using sequential cardiac- and respiratory-gated average segmented microscopy is illustrated in Fig. 6. A sequence of images of a heart stained with lectin (for vasculature) and DAPI (for nuclei), acquired over time is shown. All segments corresponding to the same phase of the cardiac and respiratory cycle, determined by the timing window $T_{GW}$, are identified and merged over time. The total acquisition time is thus dependent on segment accumulation, which continues until the merged views are all averaged the same number of times. Each view in the final reconstructed image corresponds to an average of 7 different images. From the reconstruction, it is clear that there is a marked difference between the original and merged images, with the final reconstructed image exhibiting significantly higher SNR. We emphasize that the same results can be obtained in the prospective acquisition modality as well. From a reconstruction point of view, there is no difference between which acquisition modality is being used as motion is reproducible. The only difference using a prospective modality, is that raw image acquisition is triggered at specific time points Fig. 1(c) while in the retrospective mode the collection is done after the acquisition has been made (Fig. 1(d)). This implies that the number of raw images that are necessary to be acquired is typically fewer in prospective modality as compared to the retrospective approach.

#189045 - $15.00 USD Received 13 May 2013; revised 5 Aug 2013; accepted 6 Aug 2013; published 9 Sep 2013

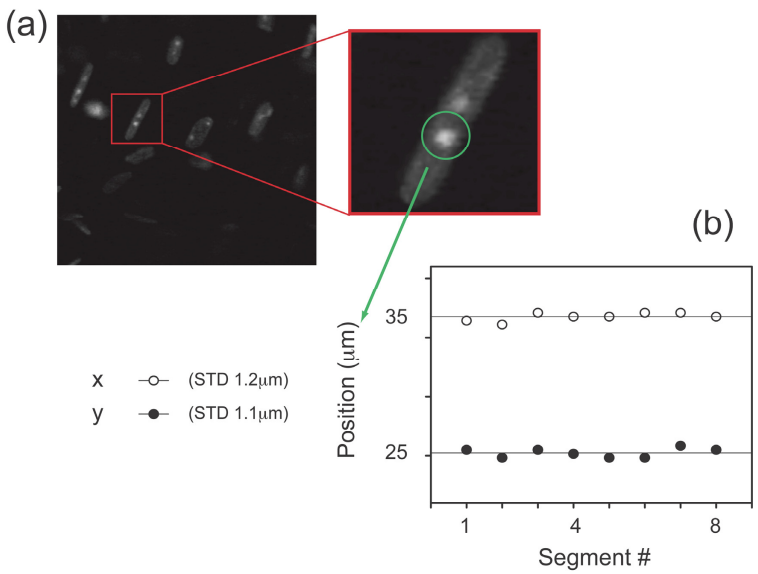


Fig. 7. (a) Stabilized image of fluorescently labeled myocyte nuclei (Hoechst 33258). Within the nuclei, subnuclear structures are clearly identifiable, and their locations were used to determine the stabilized imaging resolution (i.e. their position reproducibility over time). (b) The planar position coordinates of the labeled nucleoli shown in (a) (green circle) are plotted for different consecutive segments. The graph shows that the position of the nucleoli in each image was very stable with only a 1.2 and 1.1 micron standard deviation for the x and y coordinates, respectively. This reproducibility, which is the combined result of using the stabilizing holder in conjunction with physiological gating, makes it possible to perform sequential averaged segmented microscopy. STD, standard deviation.

The disadvantage in using a prospective approach is that not all imaging systems offer the capability to perform acquisition at a reasonably fast rate in triggered mode. For segmented gated imaging, reproducibility of motion is critical, particularly when imaging at higher magnifications. To demonstrate this, we collected a sequence of images using a time window corresponding to a segment containing a myocyte (Fig. 7(a)). The coordinate of the planar position of the nucleolus within the nucleus was monitored over several cardiac cycles, and this is plotted as a function of sequential gating in Fig. 7(a)). Our results demonstrated that the position of the nucleolus remains very stable over time, with only a 1.2 and 1.1 micron standard deviation for the planar x and y coordinates, respectively. With this degree of reproducibility, it is thus possible to perform sequential cardiac- and respiratory-gated average segmented microscopy even at high magnifications. In Fig. 8, we show a merged sequence of individually triggered segments collected over time, according to the acquisition scheme described in Fig. 3. At each step, the SNR of the reconstructed image can be seen to increase without any loss in resolution. To better characterize the sequential improvement in the SNR we calculated the standard deviation of the noise for each individual averaged image (from left to right in Fig. 8: 14.7, 10.0, 8.7, 7.6).

The approach is thus well suited to imaging scenarios where the fluorescence signal is poorly distinguishable from background noise, or where the use of high illumination power may lead to severe bleaching and phototoxicity (which preclude imaging over time).

## 6. Conclusion

In conclusion, we present a novel imaging scheme for cardiac- and respiratory-gated sequential average segmented microscopy that produces high SNR motion-artifact-free *in vivo* heart imaging. The methodology described here is similar to that currently used for cardiac MRI and is analogous to the 'segmented K-space filling' strategy. With the use of a

#189045 - $15.00 USD Received 13 May 2013; revised 5 Aug 2013; accepted 6 Aug 2013; published 9 Sep 2013

previously developed stabilizer that ensures reproducibility in motion over time, we demonstrate that our technique produces high SNR images from low SNR data. This is extremely valuable for high-speed image acquisition, or for scenarios where the fluorescence signal is not significantly higher than background noise e.g., where there is low intrinsic endogenous or exogenous fluorescence.

An important limitation, however, is that high-speed motion components during certain cardiac phases are not amenable to high resolution multiphase ECG-triggered cardiac imaging. It is therefore not possible to obtain an analogue of an MRI dynamic (Cine)-sequence [16], which is based on the quasi-periodicity, and reproducibility of the cardiac motion. In this MRI modality complete k-space images can be reliably reconstructed by grouping segments acquired at different times within a defined period of the cardiac cycle in the ECG, i.e. within a cardiac phase. Thanks to the relatively low resolution of the MR images, the whole R-R period (except the duration of the R wave) can be used for acquisition. The R-R period can then be subdivided in N intervals and N repeated segments of the k-space can be acquired within each interval. The whole k-space matrix can be then reconstructed by

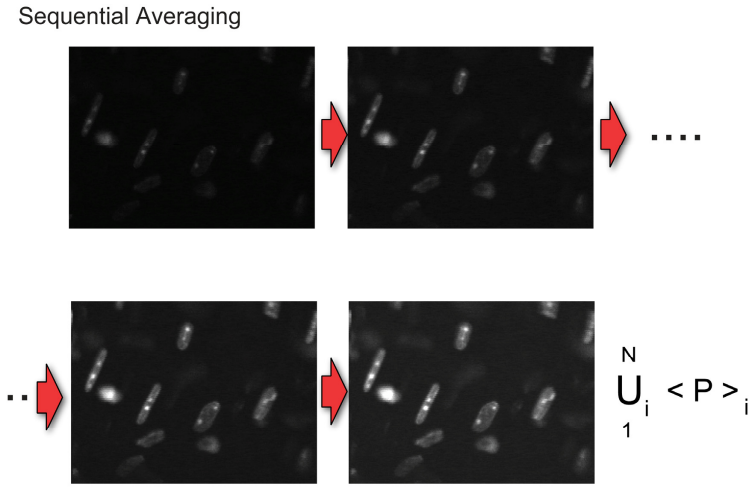


Fig. 8. Retrospectively gated sequential average segmented microscopy images of fluorescently stained cardiac myocytes (nuclear stain: Hoechst 33258). Left to right: individually triggered segments are summed over time, following the scheme in Fig. 3. For convenience of display, images are not normalized but presented as a sum and displayed on the same scale. The standard deviation of the noise was calculated for each individual averaged image (from left to right: 14.7, 10.0, 8.7, 7.6).

grouping segments according to their temporal point within the R-R time interval to obtain N images of the same slice at different cardiac phases. The N images of the selected slice can be then reconstructed as a Cine loop to reveal the dynamics of the cardiac cycle. When imaging at the cellular level such is the case herein using confocal microscopy, a Cine strategy is not feasible. Nevertheless, the frequency components of individual segments can still be easily obtained and used to characterize size features at different time points. Going forward, we envision that this feature could be exploited to obtain structural information at the cellular level across an entire cardiac cycle.

**Acknowledgments**

This project was funded in part by Federal funds from the National Heart, Lung, and Blood Institute, National Institutes of Health, Department of Health and Human Services (under Contract No. HHSN268201000044C), and from the Institute of Biomedical Engineering (R01EB006432), and National Institutes of Health P01 AI54904.